1   **Article**

2

3

4

5

6

7   **Neural correlates of conscious visual perception lie outside the visual system: evidence from**

8   **the double-drift illusion**

9   Sirui Liu[1,*,†], Qing Yu[1,2,†], Peter U. Tse[1], Patrick Cavanagh[1,3]

10

11   [1]Department of Psychological and Brain Sciences, Dartmouth College, Hanover, NH 03755,

12   USA

13   [2]Department of Psychiatry, University of Wisconsin-Madison, Madison, WI 53719, USA

14   [3]Department of Psychology, Glendon College, Toronto, ON, M4N 3M6, Canada

15

16   [†] Co-first authorship

17   * Correspondence and lead contact: Sirui.Liu.GR@dartmouth.edu

18

19

20

21

22

23

24

25

26   **Summary**

27   When perception differs from the physical stimulus, as it does for visual illusions and binocular

28   rivalry, the opportunity arises to localize where perception emerges in the visual processing

29   hierarchy. Representations prior to that stage differ from the eventual conscious percept even

30   though they provide input to it. Here we investigate where and how a remarkable misperception

31   of position emerges in the brain. This "double-drift" illusion causes a dramatic mismatch between

32   retinal and perceived location, producing a perceived path that can differ from its physical path by

33   45˚ or more [1]. The deviations in the perceived trajectory can accumulate over at least a second

34   [1] whereas other motion-induced position shifts accumulate over only 80 to 100 ms before

35   saturating [2]. Using fMRI and multivariate pattern analysis, we find that the illusory path does

36   not share activity patterns with a matched physical path in any early visual areas. In contrast, a

37   whole-brain searchlight analysis reveals a shared representation in more anterior regions of the

38   brain. These higher-order areas would have the longer time constants required to accumulate the

39   small moment-to-moment position offsets that presumably originate in early visual cortices, and

40   then transform these sensory inputs into a final conscious percept. The dissociation between

41   perception and the activity in early sensory cortex suggests that perceived position does not emerge

42   in what is traditionally regarded as the visual system but emerges instead at a much higher level.

43

44   **Keywords**: motion-induced position shift; conscious perception; frontal cortex; MVPA

45

46   **Introduction**

47   The representation of location is determined by an object's current retinal location in

48   combination with several other sources of information, such as head and eye directions [3-6], eye

49   movement plans [7], and the object's own motion [8]. Studies have shown that our visual system

50   can predict the current location of a moving target by taking into account its velocity and the neural

51   delays between the retina and the cortex [9]. This predictive position shift, extrapolating the target

52   ahead along its motion path, was proposed to underlie several motion-induced position shifts in

53   which an object's location appears to be shifted by surrounding motion signals or by its own

54   motion [8,10-13].

55   The goal of the present study is to use predictive position shifts to investigate where the

56   representation of perceived position emerges in the processing hierarchy. We used a probe that

57   induces a remarkably large motion-induced position shift, namely, the double-drift illusion [1,14-

58   16]. Compared with other well-known motion-induced position shifts, this stimulus reveals an

59   integration of motion signals over a second or more, leading to dramatic shifts in perceived

60   position that can deviate from the physical motion trajectory by many visual degrees (**Figure 1**

61   and **Movie S1**). With such a long integration period, it is unlikely that early visual areas with

62   their short integration time constants are responsible for the accumulation of position errors

63   underlying this illusion. Thus, the double-drift stimulus presents the opportunity to explore

64   where in the visual processing hierarchy position information transitions from retinally-based,

65   bottom-up encoding, to high-level, motion-influenced perceptual representations associated with

66   visual conscious experience. Specifically, if the patterns of neural activity that encode perception

67   can be distinguished from those driven by the physical stimulus, we can identify the cortical

68   areas where the percept first arises using multivariate pattern analysis (MVPA) on fMRI signals.
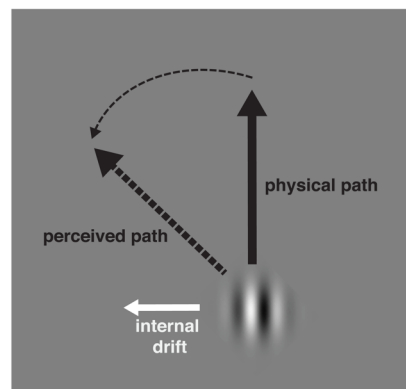

Figure 1. Double-drift stimulus.
A Gabor patch with vertical physical motion path can be perceived to be moving obliquely
if its internal texture is drifting orthogonally to its physical path. See also Movie S1.

69   The present study investigated where and how the perceived position of the double-drift

70   illusion is encoded in the brain using fMRI and MVPA. We found that the illusory motion paths

71   of two double-drift stimuli with identical retinal but different perceived paths can be decoded from

72   multiple brain regions, but the nature of the representation differs in these brain areas: activation

73   patterns for the illusory motion paths were decodable in V2 and V3 but not in V1 or MT+. However,

74   cross-classification between the double-drift and control stimuli with matched physical motion

75   paths showed no evidence that the pattern of response to the illusory paths in these areas was

76   related to the response to their matched physical paths. In contrast, a whole-brain cross-

77   classification searchlight analysis revealed that activations in more anterior parts of the brain share

78   a common position encoding for the illusory and matched physical path of the double-drift

79   stimulus with no such shared representation observed in early visual areas. That is, only in higher-

80   order brain areas did the neural coding reflect the similarity in perception of the illusory and

81   matched physical paths. Thus, our results indicate that different cortical regions are involved in

82   representing different properties of the double-drift stimulus, with the early retinotopic visual areas

83   V2 and V3 possibly generating the local direction deviations driven by motion signals integrated

84   over short durations and the higher-order regions possibly accumulating and storing position

85   displacements based on extrapolations of those integrated motion directions to represent the long-

86   lasting perceived motion path that can deviate from its physical path by 45˚ or more.

87

88   **Results**

89   *Perceived path orientation of the double-drift stimulus deviates largely from its physical path*

90   *orientation*

91   We first conducted a behavioral task to measure the size of perceived position shift of the

92   double-drift stimulus for each participant (see **Figure 2A** and **STAR Methods** for details). As

93   expected from previous literature, the perceived path orientation of the double-drift stimulus was

94   significantly different from that of the control stimulus that lacked internal motion (perceived

95   rightward tilt: $p < .001$, Cohen's $d = 13.42$; perceived leftward tilt: $p < .001$, Cohen's $d = 14.89$).

96   Specifically, the perceived path orientation was biased toward its internal drift direction,

97   suggesting that there was a consistent motion-induced position shift of our double-drift stimuli

98   across all subjects (average illusion size = 47.55˚). There was no significant difference in the

99   absolute amount of perceived direction shift between the two internal drift conditions (i.e.

100   leftward vs. rightward tilt) of the double-drift stimulus ($p = .67$, Cohen's $d = .23$).
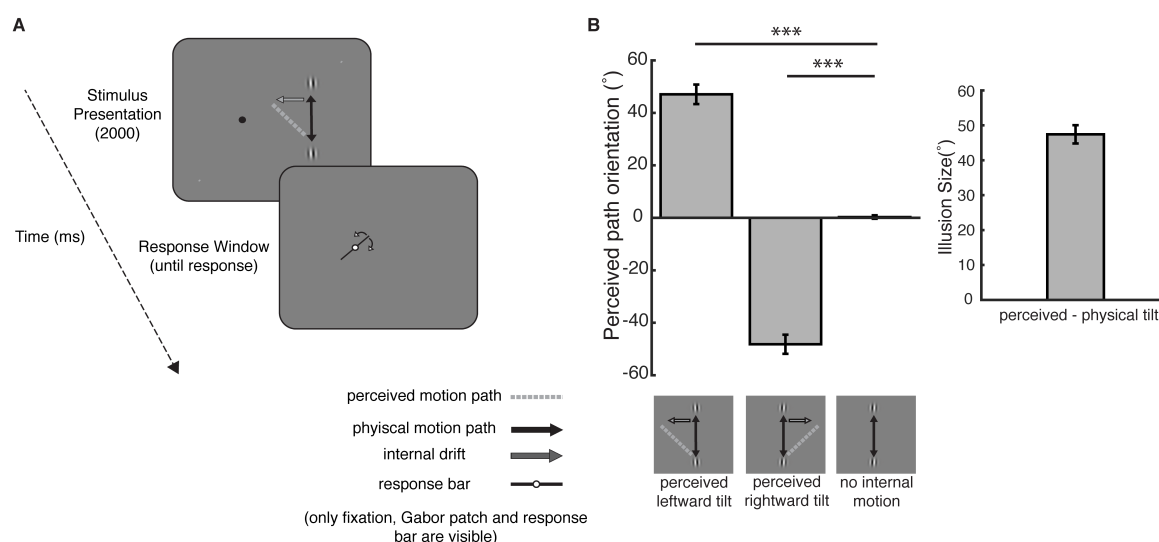
101

Figure 2. Behavioral task trial sequence and performance.
(A) Each trial began with a Gabor patch shown in the right hemifield moving vertically (example stimulus is a double-drift stimulus with a possible perceived motion path tilted leftward driven by its internal motion) for 2 seconds which then disappeared. A response bar then appeared at fixation and remained on the screen until participants adjusted its orientation to the perceived motion path of the Gabor patch.
(B) Group averaged perceived path orientation (°) of the double drift stimulus and control stimulus (no internal drift) and the illusion size of the double-drift effect. Error bars represent 95% CI.

102 *Perceived paths are decodable in V2 and V3 but do not share the same activation patterns with*

103 *that of matched physical paths*

104   We then used fMRI and MVPA to classify the activation patterns driven by a double-drift

105 stimulus that moved along the same physical path but could produce two illusory paths with

106 opposite perceived orientations depending on the direction of its internal drift motion.

107 Importantly, as the internal drift of the double-drift stimulus reverses its direction at the two

108 endpoints of the motion path, both illusory trajectories have equal periods of leftward and

109 rightward local motion across a complete back and forth cycle, so the only difference between

110 the two conditions is their perceived motion direction. We compared these perceived motion

111 paths with those of matched Gabor stimuli, lacking internal drift motion, that physically moved

112 in the direction of the two illusory paths as measured in the behavioral task for each subject (see

113 **STAR Methods** for details). The MVP classification analysis was first conducted in voxels that

114 showed significantly greater BOLD responses to the motion path locations within each of the

115 early visual areas defined in a separate retinotopic mapping session. **Figure 3A** shows these 4

116 motion path ROIs (MPROIs) for V1, V2, V3, and MT+ on a representative participant (see

117   **Table S1** for ROI sizes). When training the linear SVM classifier and testing on the left-out

118   dataset from the same stimulus conditions, classification accuracies for the two control stimuli

119   (physical leftward vs. rightward path orientation) were significantly above chance in all 4

120   MPROIs ($ps < .001$; p values were adjusted using FDR method in this and all subsequent

121   analyses; **Figure 3B;** See **Table S1** for statistical results). This suggests that the activation

122   patterns for the two stimuli with physical path orientations that matched those of the perceived

123   path of the double-drift stimulus can be reliably differentiated in these retinotopic visual areas.

124   However, classification accuracies for the two double-drift stimuli (illusory leftward vs.

125   rightward path orientation) were significantly above chance only in area V2 ($p = .004$) and V3 (p

126     $< .001$) but not in V1 ($p = .44$) or MT+ ($p = .12$) (**Figure 3B;** See **Table S1** for statistical

127   results). This indicates that activity in V2 and V3 differed for the two perceptual motion paths of

128   the double-drift stimulus whereas activity in V1 were indistinguishable for these two perceptual

129   conditions. This is consistent with a recent study that finds evidence for the involvement of

130   retinotopic areas with anatomically separated quadrantic representation of visual space, such as

131   area V2 and V3, in deriving the illusory motion of this stimulus [17]. In addition, our results
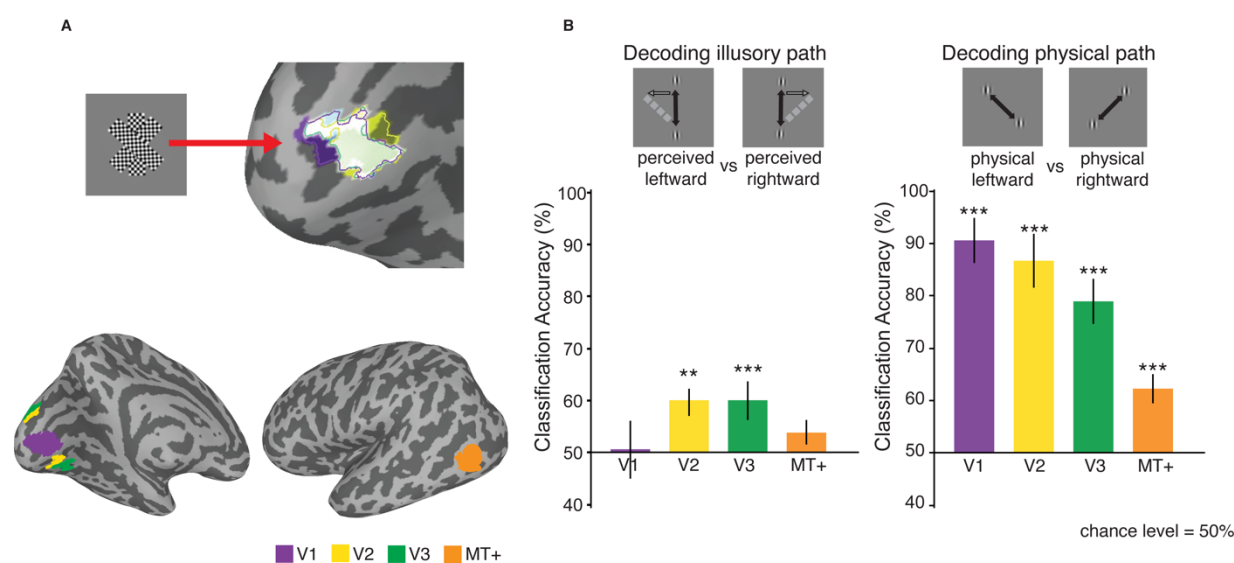

Figure 3. MPROIs and decoding accuracy.
(A) Voxels for MPROIs were selected within each early visual area by combining regions that showed greater activation for any of the three tilted checkerboard rectangles than to fixation. Example ROIs shown in a representative participant: V1 (purple), V2 (yellow), V3 (green), and MT+ (orange).
(B) Classification accuracies on the two double drift stimuli (perceived rightward vs. leftward motion path) and the two control stimuli (physical rightward vs. leftward moth path) in the MPROIs of V1, V2, V3 and MT+. Error bars represent ± 1 SEM, ** $p < .01$, *** $p <.001$. See also Figure S3 and Table S1.

132   show that the activity pattern in MT+ did not correspond to the two perceived motion paths for

133   the double-drift stimulus. This is surprising since there is evidence that suggests that neurons in

134   MT+ represent the perceived position offsets driven by motion signals [18-20]. However, since

135   the physical position was also not encoded as strongly in MT+ as in other early visual regions,

136   e.g. V1-V3, it is possible that the lack of perceived position information in MT+ for this stimulus

137   was due to weak position signals in this region.

138   To directly examine whether the activation patterns for the illusory motion paths of the

139   double-drift stimulus share a similar structure with those of the matched physical motion paths,

140   we conducted a cross-decoding analysis where we trained the linear SVM classifier with the data

141   corresponding to the two double-drift stimuli and tested with the data corresponding to the two

142   control stimuli, as well as the reverse analysis where we trained the classifier on the control

143   stimuli and tested on the double-drift stimuli. Interestingly, classification accuracies from cross-

144   classification in either direction were not significantly different from chance in any of the

145   MPROIs ($p > .1$; See **Table S1** for statistical results), including V2 and V3. Thus, although the

146   activation patterns of the two double-drift stimuli can be differentiated in V2 and V3, their

147   representations carried different information from those of their matched physical motion paths

148   in these two areas.

149

150   *Representational structure in early visual areas reveals strongest dissimilarity between physically*

151   *different motion paths*

152   Since the previous analysis suggested different representations of illusory and physical

153   motion paths in these early visual cortices, we further conducted representational similarity

154   analysis (RSA) to examine the representational structure of the five stimulus conditions in the early

155   visual MPROIs [21]. **Figure 4** shows the dissimilarity matrices (DSMs) of the five stimulus

156   conditions V1, V2, V3 and MT+. Early visual areas V1-V3 exhibited the strongest dissimilarity

157   between the stimuli with different physical motion paths (physical left path vs. rightward vs.

158   vertical motion path) as compared to those that shared the same physical motion direction but with

159   a large perceptual difference (double-drift stimuli: illusory leftward vs. rightward) (V1: $r = 0.91$,

160   $p = .001$; V2: $r = 0.81$, $p = .016$; V3: $r = 0.70$, $p = .05$). This similarity structure confirmed that the

161   representation of the double-drift stimulus in these early visual areas was largely influenced by its

162 physical motion path. The representational structure in MT+ showed high similarity between all
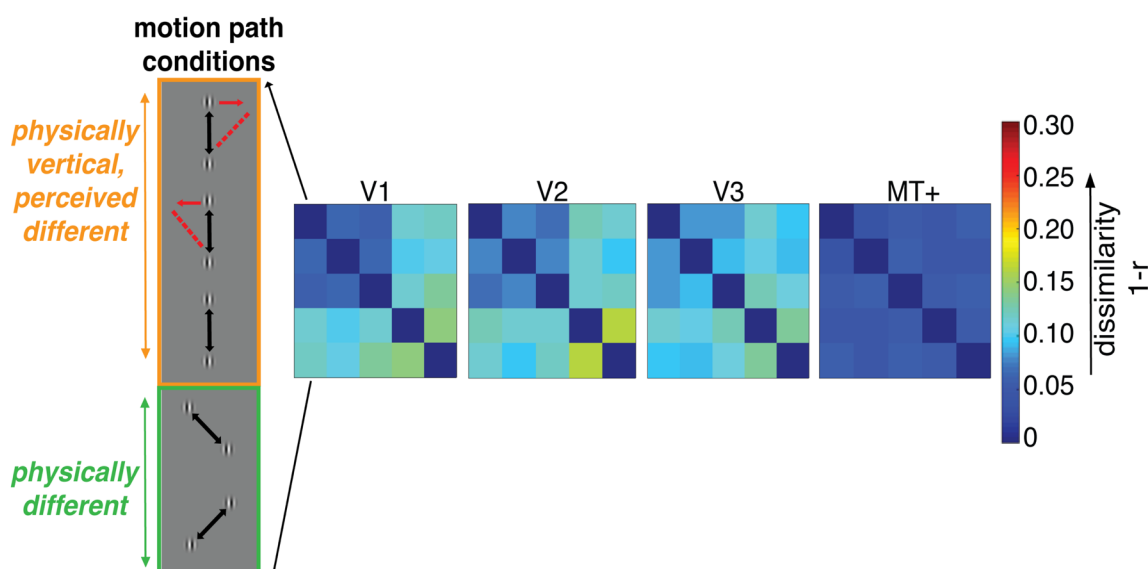163 stimulus conditions (r = 0.27, *p* = .5).

Figure 4. Results of the representational similarity analysis (RSA).
Representational dissimilarity matrices for the five stimulus conditions in MPROIs (V1, V2, V3 and MT+).

164

165 *No difference in BOLD response amplitude between illusory and matched physical paths*

166 We also calculated BOLD signal changes of each stimulus condition relative to baseline
167 within each MPROI to examine whether the above-chance decoding accuracies for the illusory
168 and physical motion paths from MVPA could be detected at the univariate level. Group averaged
169 BOLD time courses corresponding to the illusory and matched physical motion conditions from
170 each MPROI are shown in **Figure S3**. All early visual MPROIs exhibited above-baseline activity
171 for the five stimulus conditions (*p*s < .05) except V1, which showed above-baseline activation only
172 for the control stimulus with leftward motion direction (*p* < .05). Importantly, we observed no
173 difference in response magnitude for the two double-drift stimuli (*p*s > .1), or for the two control
174 stimuli with matched physically different motion paths in these MPROIs (*p*s > .1), suggesting that
175 the above-chance decoding accuracies in these regions from MVPA cannot be simply explained
176 by differences at the aggregate activation level. In addition, there was no significant difference in
177 mean signal intensity between the double-drift and the control stimulus that had the same physical
178 path direction but differed in the presence of internal motion in any of these MPROIs (**Figure S3C**;

179   ps > .1), suggesting that the two conditions were matched in terms of stimulus energy. Thus, the

180   failure in cross-decoding in these regions was not simply due to a mismatch of internal motion in

181   the double-drift and control stimulus.

182

183   *Higher-order regions show a shared representation of the illusory and matched physical motion*

184   *paths*

185   Our classification results showed that the illusory motion path can be reliably decoded in

186   some of the early visual MPROIs. To further explore areas in the brain that could decode the

187   illusory motion paths beyond the pre-defined visual ROIs, we conducted a whole-brain searchlight

188   analysis using a 4-voxel radius spherical searchlight. The same decoding analyses for the illusory

189   and matched physical paths as for the ROI-based analysis were conducted, and results of the

190   searchlight analysis were corrected using a cluster thresholding method for multiple testing (see

191   **STAR Methods** for details). **Figure 5** shows the group accuracy maps from the classification

192   searchlight analysis for decoding the illusory motion paths (**Figure 5A**) and the matched physical

193   paths (**Figure 5B**). We identified several clusters in the two hemispheres that showed decoding

194   accuracies that were significantly higher than chance levels for the illusory motion path outside

195   our pre-defined early visual ROIs: a large cluster that spans the superior frontal and medial frontal

196   gyrus, and several clusters in the superior temporal gyrus, dorsal anterior cingulate cortex, and the

197   left postcentral gyrus. We also found a cluster spanning the early visual cortex that confirmed our

198   significant decoding results in the ROI-based analysis (see **Table S2** for a complete list of

199   significant clusters). Decoding the matched physical motion paths yielded an even larger range of

200   cortical regions, including visual, parietal, and frontal areas (**Table S2**).

201   Our ROI-based cross-decoding results showed that the activation pattern for the double-

202   drift stimulus had little or no similarity to that of its matched physical motion path in any of the

203   localized regions of the early visual areas. It is however possible that a shared encoding of the

204   illusory and matched physical motion path of the double-drift stimulus is represented somewhere

205   outside our pre-defined visual ROIs. This shared encoding could be a marker of the emergence of

206   the perceptual, as opposed to the retinal, location of the double-drift stimulus. We therefore also

207   conducted a whole-brain searchlight analysis using a cross-decoding classifier between the double-

208   drift and control conditions to further explore the locus of any such shared representations. The

209   results of this searchlight analysis should yield regions with similar patterns of activation for the

210   double-drift and control stimulus that have the same perceived orientation. Interestingly, we found

211   several significant clusters in anterior parts of the brain that have above-chance cross-decoding

212   between the illusory and matched physical paths (**Figure 6;** see **Table S3** for a complete list of

213   significant clusters) but, in agreement with the previous ROI analysis, none in early visual areas.

214   Specifically, we found clusters that had above-chance cross-decoding in both directions (i.e.

215   trained on double-drift then tested on control stimuli and trained on control then tested on double-

216   drift stimuli) in the anterior cingulate and medial frontal gyrus in both hemispheres, anterior part

217   of the middle frontal gyrus in the left hemisphere, left inferior parietal lobule and parahippocampal

218   gyri. Besides these overlapping regions, cross-decoding from double-drift to control stimuli

219   resulted in additional significant clusters in the middle and inferior frontal gyrus and medial frontal

220   gyrus in both hemispheres; cross-decoding from control to double-drift stimuli produced additional

221   significant clusters in the right precentral gyrus and left parahippocampal gyrus. In addition to

222   these cortical clusters, we also found several subcortical clusters as detailed in **Table S3.**

223   To exclude the possibility that the failure in cross-decoding in regions such as the early

224   visual cortex was caused by (potentially) subtle difference in mean signal intensity across

225   conditions, even though their differences in mean activation amplitude were not statistically

226   significant (**Figure S3**), we performed an additional searchlight analysis where we removed the

227   grand mean of each stimulus condition within each searchlight. The results remained qualitatively

228   similar to that of the original cross-decoding searchlight analysis as shown in **Figure 6**, with no

229   significant clusters observed in early visual cortex (see **Figure S4** and **Table S4**). This suggests

230   that failure in cross-decoding in regions such as the early visual cortex was not simply due to a

231   difference in stimulus-driven responses between stimulus conditions of the training (e.g. physical

232   leftward vs. rightward paths) and testing dataset (e.g. illusory leftward vs. rightward paths).
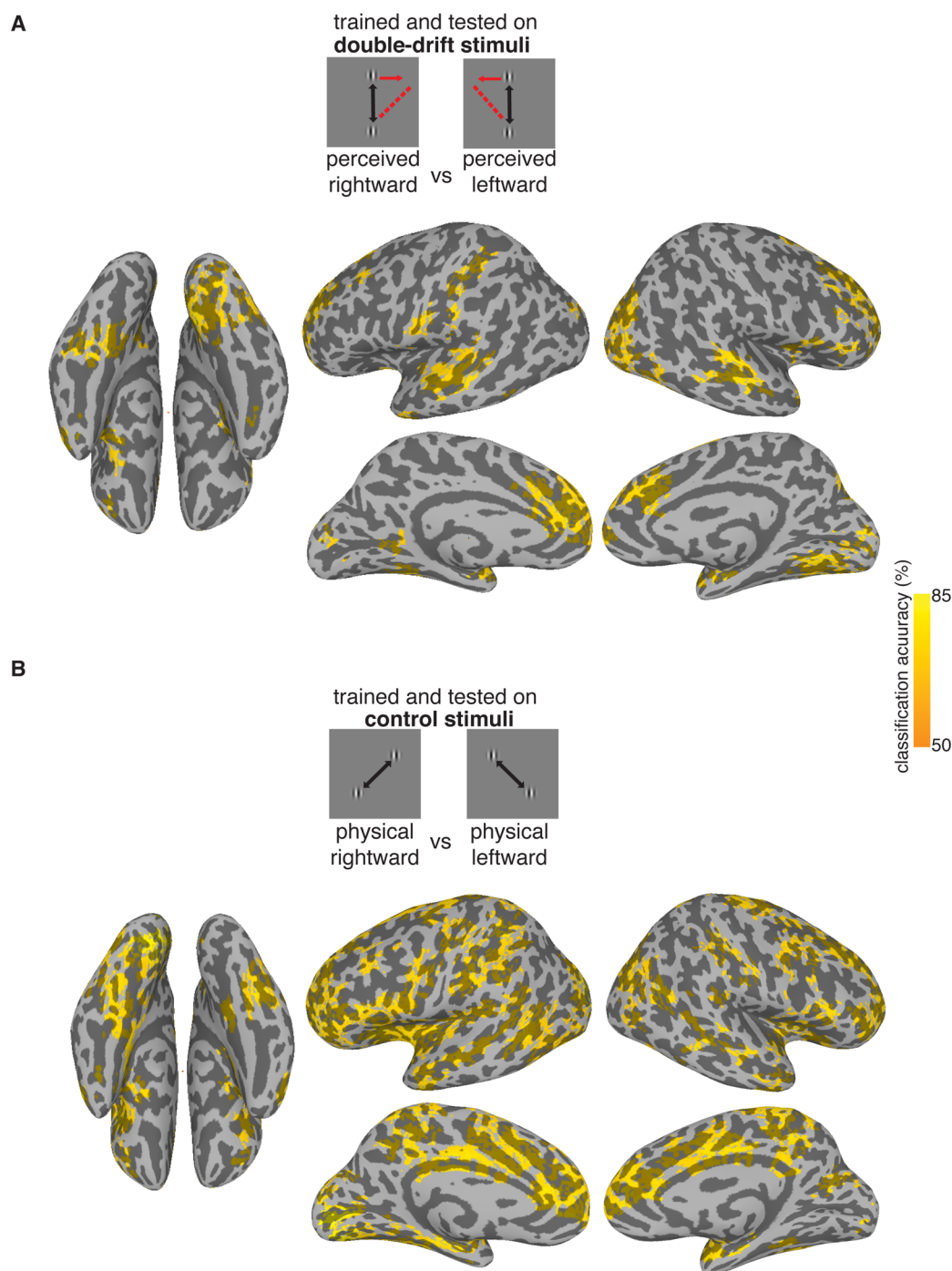
Figure 5. **Group accuracy maps of the within-condition classification searchlight analysis.**
(A) Decoding the illusory motion paths.
(B) Decoding the matched physical motion paths.
Results were thresholded at $p = .01$ and FDR corrected across clusters at $p < .05$. See also Table S2.
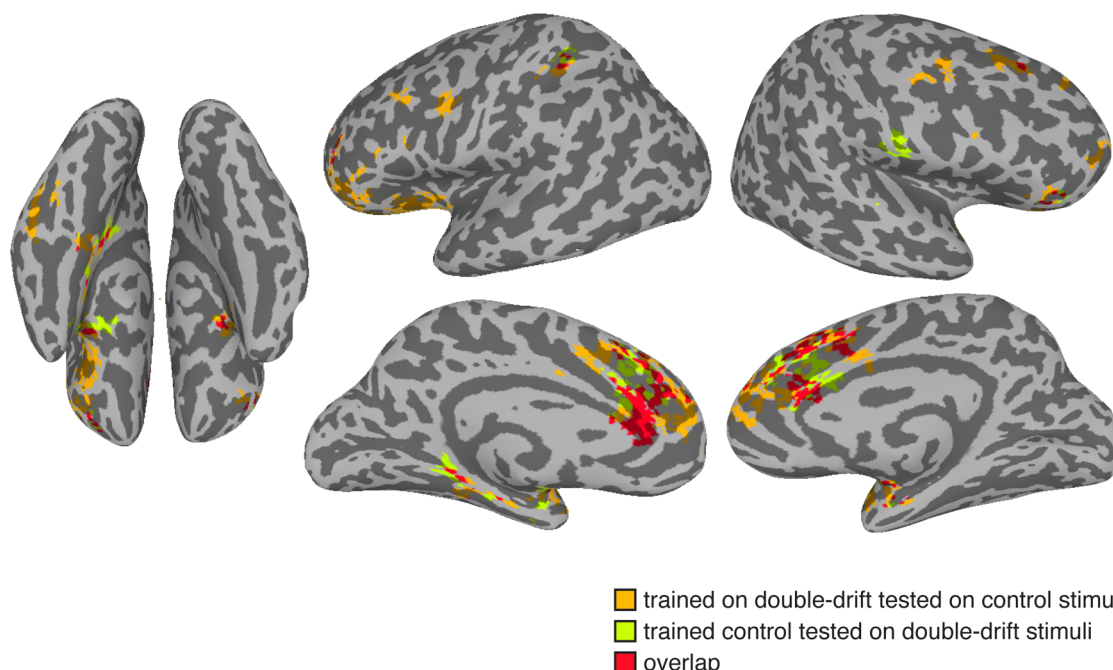
233

□ trained on double-drift tested on control stimuli
□ trained control tested on double-drift stimuli
□ overlap

Figure 6. **Cluster-thresholded searchlight map with significant above-chance cross-decoding accuracy.**
Orange represents significant clusters when training the classifier on double-drift and tested on the control stimuli. Green represents significant clusters when training the classifier on the control and tested on the double-drift stimuli. Results were thresholded at $p = .01$ and FDR corrected across clusters at $p < .05$. See also Figure S4 and Table S3 and Table S4.

234

235   **Discussion**

236   The aim of this experiment was to localize areas of cortex associated with perceived object

237   positions and trajectories when they differ from the positions and trajectories registered on the

238   retina. Normally, the location of retinal input and the corresponding perceived positions are well

239   matched, but in a remarkable motion-induced position shift, the 'double drift' illusion, there is a

240   dramatic mismatch between physical and perceived position. In particular, the perceptual

241   displacement can be as large as several degrees of visual angle and can build for a second or more

242   [1].

243   Although we found that the perceived motion path of the double-drift stimulus can be

244   decoded in early visual areas V2 and V3, results from cross-classification analysis reveal that the

245   activation patterns that differentiated the illusory motion paths in these early visual regions were

246 not related to the activity patterns that encoded the physical motion paths with matched perceptual

247 orientation. Therefore, the basis of our classification results in these early regions is likely not

248 related to the perceived motion path *per se* but might arise from lower level properties of the

249 stimulus such as the combined vector of the local and global motion. For example, leftward internal

250 drift was associated with an upward external motion in one case (e.g. double-drift stimulus with

251 perceived leftward trajectory), and with a downward external motion in the other (e.g. double-drift

252 stimulus with perceived rightward trajectory).

253   Interestingly, the significant cross-classification clusters found in our searchlight analysis

254 were primarily in areas that are known to be involved in executive control, such as the lateral

255 prefrontal cortex (LPFC) [22,23], dorsal anterior cingulate (dACC) (the cingulo-opercular control

256 network; [24,25]), pre-supplementary motor area (preSMA) [26] and medial prefrontal cortex

257 (MPFC) [27], and in spatial information processing such as the inferior parietal lobule (IPL)

258 [28,29]. This indicates that the neural coding for the perceived motion path in these high-order

259 regions was driven by a representation of the illusory motion path that was similar enough to that

260 of the matched physical motion path to permit cross-decoding. Importantly, these regions have

261 been implicated in the literature in transforming sensory representations to different

262 representational formats for different functional purposes. For example, lateral frontal regions have

263 been implicated in forming abstractions of incoming information [30,31]. Motor-related areas such

264 as preSMA are involved in encoding past and current information for perceptual decision making

265 and generating motor preparatory signals from readout of sensory information [32-34]. The

266 cingulo-opercular network was shown to be involved in downstream control process for perceptual

267 recognition and working memory output gating, by integrating information accumulated from the

268 frontoparietal and sensory regions [35,36]. IPL has been implicated in transforming visuospatial

269 information into motor output [37-40]. Therefore, successful cross-classification in higher-order

270 cortical regions as observed in our study may reflect similar representational changes from a

271 sensory format to a different, more abstract format, which could allow for generalization between

272 different physical stimuli in a shared format of perceptual experience.

273   In comparison, representations in early visual cortex are sensitive to stimulus-specific

274 changes and therefore may not permit successful cross-classification between the illusory and

275 matched physical motion paths. Indeed, our results show that this high-level representation of

276 perceived as opposed to real stimulus positions was not shared with or projected back down to

277   early visual areas. Instead, the observed above-chance classification in V2 and V3 for the perceived

278   motion path might suggest that activity in these areas encodes the combined motion signals

279   integrated over short durations. These local direction errors are the base data that get integrated

280   into the illusory path, but likely do not account for the illusion alone, because these errors appear

281   to accumulate over long durations, and cells in these early processing stages do not have the

282   second-long integration time windows that the double-drift stimulus requires to build up the

283   position deviations. Indeed, one distinct feature that makes this illusion such a powerful effect is

284   that its perceived motion path can be formed by accumulating position shifts over long durations

285   of a second or more, while other motion-induced position shifts effects like the flash-grab stimulus,

286   only integrate motion signals over about 90 ms [10]. Given the short decay time constant for

287   orientation cells in early visual areas [41], it is possible that a motion-position integration process

288   of such a long duration requires higher-order brain areas to store and accumulate position offsets

289   in order to form a consistent motion trajectory. Thus, our results suggest that the higher-order areas

290   where we find significant cross-classification could be candidate areas that accumulate outputs

291   from V2 and V3 so that perception continues to drift farther away from the real path for over a

292   second.

293   Our finding that there is no shared activity in early visual cortex that corresponds to the

294   physical and perceived paths conflicts with some of the previous fMRI studies of motion-induced

295   position shifts [19,42,43]. In the case of the "flash-grab" illusion where a flash is pulled forward

296   by the motion that underlies it [10], it was shown that neural activity for the perceived position

297   shifts of this stimulus correlates strongly with activity seen for physical stimuli with locations

298   matched to the illusory ones solely in early visual cortices V1 through V3 but not in higher-order

299   areas [43]. Similarly, for the related "flash-drag" illusion [44], activity in early retinotopic cortical

300   areas, most notably MT+, also shows strong correlation between perceived position of a flash that

301   was shifted by surrounding moving patterns and matched physical positions [19]. We suggest that

302   the involvement of top-down attentional signals may account for the discrepancies between these

303   results and ours. In particular, when higher-order areas generate a percept of an object, downward

304   attentional signals can feed back to early visual cortex and generate activation at locations where

305   the object is expected, rather than where it is in retinotopic coordinates [45]. These downward

306   signals would complicate any attempt to determine where perceptual representation begins as

307   activations in early cortical areas would be composed of a combination of bottom-up activations

308 matching the physical stimulus, and top-down activations that, based on the percept, matched its
309 expected location and properties. The presence of such top-down activations would support cross-
310 classification between perceived and matched physical motion paths in all areas that received such
311 feedback. Although there is not yet direct evidence that attention is extrapolated to match these
312 shifts in perceived position, it is well established that saccades are directed to the perceived rather
313 than physical locations for the motion-induced position shifts that displace the target along the
314 direction of motion, such as the flash-lag and flash-drag stimuli [46-49]. Given the close link
315 between the saccade and attention system [50,51], it is reasonable to assume that attention will be
316 shifted by these illusions to the same extent as perception and saccades.

317   For the double-drift illusion, on the other hand, saccades are directed to the physical
318 location of the stimulus, not its perceived location [1]. The dissociation of saccades and perception
319 is unique to this stimulus as other motion-induced position shifts affect saccades and perception
320 equally [46-49]. Given the immunity of saccades to the double-drift illusion, we speculate that
321 attentional shifts, like saccades, are not affected by the illusion either. If correct, any downward
322 projections from areas involved in attentional shifting circuitry would prioritize the stimulus's
323 physical locations, rather than its perceived, illusory ones. If this is the case, there would be no
324 activity at cortical regions corresponding to illusory locations prior to those areas in the visual
325 processing hierarchy that actually do encode the perceived location. Since we find no cross-
326 classification between perceived and matched physical paths in early visual areas for the double-
327 drift stimulus, we assume that either such attentional feedback is weak if it is to the perceived
328 locations, or more likely, that the top-down feedback is in fact to the physical locations. If this
329 assumption is correct, this stimulus affords the unique possibility of probing where the perceptual
330 coordinates of object position arise in the processing hierarchy without the confound of top-down
331 attentional projections. The feedback signals in this case would simply prioritize the stimulus's
332 representation in physical instead of perceived coordinates and so would not mask the point at
333 which perception deviates from the bottom up signals.

334   In summary, our data place a lower limit on where areas of the brain are located that are in
335 perceived as opposed to retinotopic coordinates. Remarkably, there was no cross-classification of
336 corresponding real and perceived motion paths in early visual areas, a finding probably linked to
337 the absence of influence of the illusion on saccades, and by inference on attentional shifts as well.
338 Without downward projections activating the perceived locations, cortical regions prior to the

339   emergence of the percept then show only the uncontaminated bottom-up activity. And this reveals

340   that the representation of perceived position likely emerges much later in the processing hierarchy

341   than in early visual cortical areas, even if early areas such as V2 and V3 provide the instantaneous

342   direction errors that are then integrated in later areas to compute the final percept. To the extent

343   that visual consciousness coincides with perceived position, our data also place clear constraints

344   on the neural correlates of visual consciousness, at least for this particular type of stimulus.

345

346   **Acknowledgments**

350

351   **Author contributions**

352   S.L., Q.Y., P.U.T. and P.C. designed the experiment. S.L. and Q.Y. conducted the experiment

353   and analyzed the data. Q.Y. contributed unpublished analytic tools. P.U.T. and P.C. supervised

354   the entire project. S.L., Q.Y., P.U.T. and P.C. wrote the manuscript.

355

356   **Declaration of interests**

357   The authors declare no competing interests.

358

359   **Figure Legends**

360   **Figure 1.** Double-drift stimulus. A Gabor patch with vertical physical motion path can be

361   perceived to be moving obliquely if its internal texture is drifting orthogonally to its physical path.

362   See also Movie S1.

363   **Figure 2.** Behavioral task trial sequence and performance. (A) Each trial began with a Gabor patch

364   shown in the right hemifield moving vertically (example stimulus is a double-drift stimulus with

365   a possible perceived motion path tilted leftward driven by its internal motion) for 2 seconds which

366   then disappeared. A response bar then appeared at fixation and remained on the screen until

367   participants adjusted its orientation to the perceived motion path of the Gabor patch. (B) Group

368   averaged perceived path orientation (˚) of the double drift stimulus and control stimulus (no

369   internal drift) and the illusion size of the double-drift effect. Error bars represent 95% CI.

370   **Figure 3.** MPROIs and decoding accuracy. (A) Voxels for MPROIs were selected within each

371   early visual area by combining regions that showed greater activation for any of the three tilted

372   checkerboard rectangles than to fixation. Example ROIs shown in a representative participant: V1

373   (purple), V2 (yellow), V3 (green), and MT+ (orange). (B) Classification accuracies on the two

374   double drift stimuli (perceived rightward vs. leftward motion path) and the two control stimuli

375   (physical rightward vs. leftward moth path) in the MPROIs of V1, V2, V3 and MT+. Error bars

376   represent ± 1 SEM, ** $p < .01$, *** $p < .001$. See also Figure S3 and Table S1.

377   **Figure 4.** Results of the representational similarity analysis (RSA). Representational

378   dissimilarity matrices for the five stimulus conditions in MPROIs (V1, V2, V3 and MT+).

379   **Figure 5.** Group accuracy maps of the within-condition classification searchlight analysis. (A)

380   Decoding the illusory motion paths. (B) Decoding the matched physical motion paths. Results

381   were thresholded at $p = .01$ and FDR corrected across clusters at $p < .05$. See also Table S2.

382   **Figure 6**. Cluster-thresholded searchlight map with significant above-chance cross-decoding

383   accuracy. Orange represents significant clusters when training the classifier on double-drift and

384   tested on the control stimuli. Green represents significant clusters when training the classifier on

385   the control and tested on the double-drift stimuli. Results were thresholded at $p = .01$ and FDR

386   corrected across clusters at $p < .05$. See also Figure S4 and Table S3 and Table S4.

387

388   **STAR Methods**

389   **1. CONTACT FOR REAGENT AND RESOURCE SHARING**

390   Further information and requests for resources and reagents should be directed to and will

391   be fulfilled by the Lead Contact, Sirui Liu (Sirui.Liu.gr@dartmouth.edu).

392

393   **2. EXPERIMENTAL MODEL AND SUBJECT DETAILS**

394   **2.1. Subjects**

395   Nine individuals from the Dartmouth College community participated in this study (5

396   females; age range: 21-32, mean age = 26.6 +- 3.1). All participants were naïve to the purpose

397   of this study and had normal or corrected-to-normal vision. Written, informed consent

398   approved by the Committee for the Protection of Human Subjects at Dartmouth College was

399   obtained from each participant prior to the first experimental session. Participants were

400   screened by the Dartmouth Brain Imagining Center fMRI Subject Safety Screening Sheet and
401   received a compensation of $20/hour.

402

403   **3.   METHOD DETAILS**

404   **3.1. Stimuli**

405   All stimuli were generated using Matlab 2015a [52] and PsychToolbox-3 [53]. The
406   stimulus in the behavioral and the main fMRI experiment was based on the double-drift
407   stimulus used in [1] (see **Figure 1** and **Movie S1**). We used a Gabor pattern (sinusoidal
408   grating within a Gaussian envelope) with a spatial frequency of 0.5 cycle/dva (cycles per
409   degree of visual angle) and 100% contrast presented on a uniform gray background (53
410   cd/m^2). The standard deviation of the contrast envelope was 0.4 degree of visual angle
411   [dva]. The Gabor pattern moved back and forth along a linear path of length 5 dva, with a
412   speed of 5 dva/sec (external motion). The sinusoidal grating had the same orientation as
413   the motion path, and drifted in the orthogonal direction with a temporal frequency of 4 Hz
414   (internal motion), reversing direction at the two endpoints every 1 second ('double-drift
415   stimulus'), or stayed static during the trial ('control stimulus'). The midpoint of the
416   trajectory was placed at 5 dva to the right of the screen center. A black fixation point (0.3
417   dva diameter) was presented at 3 dva horizontal to the left of the screen center throughout
418   all the behavioral and MRI experiments. We moved the fixation to this location so that our
419   stimulus was 8 dva away from fixation. This was the eccentricity at which [1] found a large
420   perceptual effect. In the pre-scan behavioral task, participants reported the perceived
421   orientation of the motion path using a black line ('response bar') centered at fixation that
422   was 0.05 dva in width and 5 dva in length.

423

424   **3.2. Pre-scan behavioral task**

425   Stimuli were presented on an Apple iMac Intel Core i5 (Cupertino, CA) and were
426   displayed in a dark room on a 16'' ViewSonic G73f CRT monitor (1024 x 768 pixels at
427   90-Hz) placed 57-cm from the participant with their head stabilized on a chinrest during
428   the experiment. **Figure 2A** shows a sample trial of the pre-scan behavioral task.
429   Participants were instructed to keep their gaze at the fixation point throughout the
430   experiment. In each trial, a Gabor patch was shown in the periphery and moved back and

431 forth in a vertical path for 2 s. Its internal texture drifted either leftward, rightward or

432 remained static. For each participant, the drift direction of the internal texture was

433 randomized across trials. Following the stimulus, participants were instructed to rotate the

434 response bar by pressing the corresponding keyboard keys (up arrow for counterclockwise;

435 down arrow for clockwise) until its direction matched the perceived angle of the motion

436 trajectory of the Gabor. The response bar was presented at a random orientation for each

437 trial and remained on the screen until participants were satisfied with their response and

438 pressed the space bar for the next trial. Overall, each participant completed ten adjustment

439 trials for each internal drift direction for a total of 30 trials that lasted about 15 minutes.

440

441 **3.3. MRI acquisitions**

442 The scanning was conducted on a 3T MRI scanner (Philips Intera Achieva) with a 32-

443 channel head coil at the Dartmouth Brain Imaging Center at Dartmouth College. For each

444 subject, we collected functional BOLD activity using an echo-planar imaging (EPI) sequence

445 (TR = 2 s, TE = 35 ms, voxel size = 3 × 3 × 3 mm, flip angle = 90˚, FOV = 240 × 240 mm)

446 and a high resolution anatomical scan using T1-weighted MPRAGE sequence at the end of

447 each scanning session (voxel size = 1 × 1 × 1 mm).

448

449 **3.4. Main experiment runs**

450 Stimuli were presented on a screen (47.5 cm width) at the back of the scanner through

451 an LCD projector. The screen resolution was 1024 × 768 pixels with 60 Hz refresh rate. The

452 projected stimuli were viewed through a mirror located on the head coil with a viewing distance

453 of 101.6 cm. Participants completed 10 fMRI main experimental runs. In each run, after an

454 initial 4 s blank fixation period, participants viewed a total of fifteen trials, each of which was

455 composed of a 11s stimulus block followed by a 15s fixation block with the order of the trials

456 randomized for each participant. Each stimulus block was composed of a Gabor patch

457 presented in the right hemifield that moved back and forth along a linear path for five

458 repetitions (2s each repetition) and then disappeared for 250 ms in between repetitions. In total,

459 each experimental run was 394s long. **Figure S1A** illustrates the five stimulus conditions used

460 in the main fMRI experiment. Participants viewed three blocks per stimulus condition in each

461 run. To make sure participants were attending to the stimulus, the contrast of the presented

462   Gabor stimulus reduced 50% randomly in each run for 200 ms and participants were asked to
463   press a response button each time they saw the change. **Figure S1B** shows a sample trial
464   sequence for the main fMRI main experiment. We also conducted two additional EPI runs
465   using a rectangular checkerboard pattern flickering at 8 Hz that covered the spatial extent of
466   the perceived and physical motion paths of the double-drift stimulus. The checkerboard pattern
467   was centered at 8 dva horizontal to the right of the fixation with its height the length of the
468   motion path of the Gabor pattern and a width the size of the Gabor stimulus. **Figure S2A** shows
469   the three conditions in the stimulus location localizer runs: vertical, leftward or rightward tilted
470   checkerboard rectangle. The two oblique checkerboard stimuli were tilted in the direction of
471   the perceived motion path for the double-drift stimulus. The tilt angle was individually
472   calculated from the responses in the pre-scan behavioral task for each subject. Each run
473   contained an initial 4s fixation block and fifteen trials, each of which was composed of a 10s-
474   stimulus block with a flickering checkerboard pattern followed by a 12s. blank fixation block.
475   There were five trials per stimulus condition for a total of fifteen trials per run with the order
476   of the blocks randomized for each participant. **Figure S2B** shows the trial protocol. To
477   maintain attention to the stimulus, participants were asked to press a response button each time
478   they saw the color of the fixation point changed.
479
480   **3.5. Region-of-interest localization runs**
481   In addition to the main experiment, participants completed a separate scanning session
482   that included a standard retinotopic mapping procedure and three MT+ localizer runs (292 s
483   each). We followed the standard retinotopic mapping procedure [54,55] by using clockwise or
484   counterclockwise rotating checkerboard wedges (flickering at 4 Hz, ten 192 s runs) to map
485   polar angle and using expanding or contracting checkerboard rings (flickering at 4 Hz, four
486   192s runs) to map eccentricity. The fixation point in our experiment was moved 3 dva
487   horizontal to the left of the center of the screen to match that of our main experiment. MT+
488   was functionally localized for each participant following the procedure from [56]. In each run,
489   participants viewed seven 16s blank fixation blocks interleaved with six 30s stimulus blocks.
490   The stimulus was composed of one hundred 0.3dva diameter black dots spanning the whole
491   visual field that either moved coherently, flickering at 30 Hz, or remain static on the screen.
492   Each of the three stimulus conditions was presented twice in each run with the order

493   randomized for each subject. For the coherently moving condition, the dots could be moving

494   rightward, leftward, vertically upward or downward, expanding, contracting, rotating

495   clockwise or counterclockwise at 7 dva/s with 100% coherence, while resetting their locations

496   every 367 ms. To make sure they were fixating, participants were asked to press a response

497   button each time they saw the color of the fixation point changed for all of the localizer runs.

498

499   **4. QUANTIFICATION AND STATISTICAL ANALYSIS**

500   **4.1. Behavioral data analysis**

501   For each participant, we first determined the perceived path angle of the double-drift

502   stimulus (with leftward or rightward perceived motion paths) and the control stimulus that

503   lacked internal motion away from the physical, vertical orientation. Paired-samples t-tests were

504   conducted using R and RStudio v.1.0.136 to compare the mean differences of the perceived

505   path orientation between the double-drift stimulus and the control stimulus with no internal

506   drift [57,58]. The magnitude of the double-drift illusion was then calculated individually by

507   taking the difference between these two measurements. A positive value of the illusion size

508   indicates that the perceived motion orientation was biased toward that of the internal drift. The

509   average of this value was then used in the following scanning session as the motion direction

510   for the control stimuli that moved obliquely with no internal drift as well as the tilt angle for

511   the checkerboard pattern in the localizer runs to define ROIs for the motion path of the stimulus

512   for each subject.

513

514   **4.2. fMRI data analysis**

515   **4.2.1. *Preprocessing***

516   Functional imaging data was preprocessed using AFNI [59]. For each participant,

517   the EPIs were first registered to the last run of each scan session and then motion corrected,

518   linearly detrended, and z-scored within each run. The anatomical images collected in the

519   first scanning session were aligned to the EPI scans of the same session. Anatomical scans

520   collected in the two localizer runs that define motion path locations in the second scanning

521   session were first aligned to that of the first scanning session before aligning to the EPI

522   scans. Localizer data were further smoothed with a 4-mm FWHM Gaussian kernel. For the

523   searchlight analysis, the EPI scans were normalized to the Talairach standard space [60].

524

4.2.2. *ROI definition*

526   The cortical surface of each participant was first reconstructed with FreeSurfer [61]

527 using the high-resolution anatomical images. All data in the localizer runs were first

528 mapped onto this cortical surface to define the ROIs. Early visual areas left V1, V2, and

529 V3 were individually drawn by hand on individual surfaces based on the phase angle maps

530 computed from data in the retinotopic mapping session. MT+ was individually defined on

531 surface based on data from the MT+ localizer runs using beta coefficient values calculated

532 from a General Linear Model (GLM) analysis that specified voxels that responded more

533 strongly to moving than to stationary dot patterns ($p < 10^{-4}$ after correcting for multiple

534 tests using false-discovery rate (FDR) [62]. To identify the voxels that responded to the

535 motion path of the double-drift and control stimulus within each of the ROIs, we then

536 selected the voxels that showed significantly greater activation for any of the three tilted

537 checkerboard rectangles than to fixation ($p < 10^{-4}$, FDR corrected) in the left hemisphere

538 and only these voxels were included for the rest of the ROI-based analysis. All these

539 surface-defined results were then individually mapped back into the volume space and

540 aligned to the EPI data of the first scanning session by aligning the anatomical scans of the

541 two sessions for subsequent analysis.

542

4.2.3. *Time course of BOLD activity.*

544   To create the time series of BOLD activity in each ROI, we averaged BOLD

545 activity in all voxels within the ROI and calculated the percent signal change in activation

546 relative to baseline for each TR of each trial. Baseline was defined as the activation of the

547 first TR of each trial. Average BOLD activity at each time point was then calculated by

548 averaging the percent signal change across trials within each condition. One-sample t-tests

549 against 0 were used to assess statistical significance above baseline for each TR within

550 each ROI for each stimulus condition at $p < 0.05$ after correcting for multiple tests using

551 FDR [62]. In addition, paired samples *t*-tests were used to compare BOLD activity between

552 1) the two double-drift stimulus conditions, 2) the two control stimulus conditions, and 3)

553 the double-drift stimulus conditions with internal motion and the vertically moving control

554   stimulus without internal motion at each time point within each ROI and significance of

555   the tests were determined at $p < 0.05$ after correcting for multiple tests using FDR [62].

556

557   **4.2.4.** *Multivariate pattern analysis (MVPA)*

558   All the subsequent analyses were performed using the PyMVPA toolbox [63]. We

559   first used PyMVPA to perform MVPA within each ROIs. For each trial, we extracted raw

560   data averaged for 6 to 14 s after trial onset (considering a 6-s of hemodynamic delay) and

561   fed the averaged data into linear support vector machines (SVMs) to implement

562   classification of stimulus conditions. We performed two types of classification analyses:

563   the first analysis was to classify between the two physically different motion paths of the

564   control stimulus, or between the two illusorily-different motion paths of the double-drift

565   stimulus, using a leave-one-run-out cross-validation procedure. To examine whether the

566   activation patterns of the double-drift stimuli resembled that of the corresponding control

567   stimuli, a second cross-decoding analysis was conducted using the same data, except that

568   the training and test data were from separate conditions (i.e., training with the data

569   corresponding to the control stimuli with matched physical motion path and testing with

570   the data corresponding to the double-drift stimuli with physically vertical but perceived

571   different motion path; and vice versa). Statistical significance of classification accuracies

572   across subjects was determined by randomly shuffling the stimulus condition labels 1000

573   times to construct null distributions for each ROI and testing for significance above chance

574   at $p < .05$ after correcting for multiple tests using false-discovery rate (FDR) [62].

575   The SVMs were further combined with a spherical searchlight procedure for whole-

576   brain classification analysis. Specifically, we applied a volume-based searchlight analysis

577   by sliding a 4-voxel-radius spherical linear SVM classifier voxel-by-voxel over the whole

578   brain. As with the ROI-based analysis, the searchlight analysis was performed for decoding

579   illusory paths, the matched physical paths, and cross-decoding using a leave-one-run-out

580   cross-validation procedure. Group-level statistical significance for the searchlight analyses

581   was determined following a cluster thresholding approach [64]: 100 permuted searchlight

582   accuracy maps were first generated for each subject by randomly permuting the stimulus

583   condition labels across trials. Then 100,000 group-average accuracy maps were computed

584   by randomly sampling from each subject's permutated maps to construct a null distribution

585   of accuracy values. These bootstrapped average maps were then thresholded at $p = 0.01$

586   per voxel and were used for cluster-forming and for constructing the null distribution of

587   cluster sizes for testing the significance of the real group-average map's clusters.

588   Significance of the test was determined at $p < 0.05$ across clusters of size larger than 30

589   voxels after correcting for multiple comparisons using the FDR [62]. The same set of

590   searchlight analyses were performed where the grand mean of each stimulus condition was

591   removed within each searchlight following the same cluster-based permutation tests and

592   multiple comparison correction methods described above. Results were projected to the

593   cortical surface reconstructed from the Talairach template [60].

594

4.2.5. *Representational similaritiy analysis (RSA)*

596   To examine the neural representational geometry of the stimulus conditions, we

597   also conducted a representational similarity analysis (RSA) [21]. This was done by

598   calculating the Euclidean distance between patterns of responses for different stimulus

599   conditions. For each ROI, a dissimilarity representational matrix (1-similarity) for the five

600   stimulus conditions was derived. We then conducted a correlation test between each of

601   these dissimilarity matrices with a hypothesized correlation pattern that corresponds to the

602   case when the stimulus conditions with physically different motion path produce strongest

603   dissimarlity (i.e. 1-similarity = 1) and those with physically same but perceptually different

604   motion path (i.e. double-drift stimuli) were least dissimilar (i.e. 1-similarity = 0). P-values

605   were then corrected for multiple tests using FDR [62].

5. DATA AND SOFTWARE AVAILABILITY

608   Custom analysis codes and fMRI data from the experiment are available upon request.

Supplemental items

Movie S1. Related to Figure 1. Double-drift stimulus. This movie shows an example of the

double-drift stimulus used in the experiment. The Gabor patch moves back and forth on a linear

vertical path at the right hemifield. When fixating at the black dot, the internal grating drifts

orthogonally toward the left as the Gabor patch moves upward and reverses its direction at the

615   path reversal. The internal motion of the Gabor patch drives its perceived path to appear tilted

616   leftward rather than vertical.

617

618   **References**

619   [1]   Lisi M, Cavanagh P. Dissociation between the Perceptual and Saccadic Localization of
620   Moving Objects. Current Biology 2015;25:2535–40. doi:10.1016/j.cub.2015.08.021.
621   [2]   Chung STL, Patel SS, Bedell HE, Yilmaz O. Spatial and temporal properties of the
622   illusory motion-induced position shift for drifting stimuli. Vision Research
623   2007;47:231–43. doi:10.1016/j.visres.2006.10.008.
624   [3]   Bremmer F, Ilg UJ, Thiele A, Distler C, Hoffmann KP. Eye Position Effects in Monkey
625   Cortex. I. Visual and Pursuit-Related Activity in Extrastriate Areas MT and MST.
626   Journal of Neurophysiology 1997;77:944–61. doi:10.1152/jn.1997.77.2.944.
627   [4]   Brotchie PR, Andersen RA, Snyder LH, Goodman SJ. Head position signals used by
628   parietal neurons to encode locations of visual stimuli. Nature 1995;375:232–5.
629   doi:10.1038/375232a0.
630   [5]   DeSouza JFX. Eye Position Signals Modulate Early Dorsal and Ventral Visual Areas.
631   Cerebral Cortex 2002;12:991–7. doi:10.1093/cercor/12.9.991.
632   [6]   Snyder LH, Grieve KL, Brotchie P, Andersen RA. Separate body- and world-referenced
633   representations of visual space in parietal cortex. Nature 1998;394:887–91.
634   doi:10.1038/29777.
635   [7]   Duhamel, Colby C, Goldberg M. The updating of the representation of visual space in
636   parietal cortex by intended eye movements. Science 1992;255:90–2.
637   doi:10.1126/science.1553535.
638   [8]   Whitney D. The influence of visual motion on perceived position. Trends in Cognitive
639   Sciences 2002;6:211–6. doi:10.1016/S1364-6613(02)01887-9.
640   [9]   Nijhawan R. Motion extrapolation in catching. Nature 1994;370:256–7.
641   doi:10.1038/370256b0.
642   [10]   Cavanagh P, Anstis S. The flash grab effect. Vision Research 2013;91:8–20.
643   doi:10.1016/j.visres.2013.07.007.
644   [11]   De Valois RL, De Valois KK. Vernier acuity with stationary moving Gabors. Vision
645   Research 1991;31:1619–26. doi:10.1016/0042-6989(91)90138-U.
646   [12]   Nijhawan R. Neural delays, visual motion and the flash-lag effect. Trends in Cognitive
647   Sciences 2002;6:387–93. doi:10.1016/S1364-6613(02)01963-0.
648   [13]   Nijhawan R. Visual prediction: Psychophysics and neurophysiology of compensation for
649   time delays. Behavioral and Brain Sciences 2008;31:179–98.
650   doi:10.1017/S0140525X08003804.
651   [14]   Tse PU, Hsieh P-J. The infinite regress illusion reveals faulty integration of local and
652   global motion signals. Vision Research 2006;46:3881–5.
653   doi:10.1016/j.visres.2006.06.010.
654   [15]   Kwon OS, Tadin D, Knill DC. Unifying account of visual motion and position
655   perception. Proceedings of the National Academy of Sciences, vol. 112, 2015, pp. 8142–
656   7. doi:10.1073/pnas.1500361112.
657   [16]   Shapiro A, Lu Z-L, Huang C-B, Knight E, Ennis R. Transitions between Central and
658   Peripheral Vision Create Spatial/Temporal Distortions: A Hypothesis Concerning the

659   Perceived Break of the Curveball. PLoS ONE 2010;5:e13296.
660   doi:10.1371/journal.pone.0013296.

661 [17]   Liu S, Tse PU, Cavanagh P. Meridian Interference reveals Neural Locus of Motion-
662   induced Position Shifts. Journal of Neurophysiology 2018;405:655.
663   doi:10.1152/jn.00876.2017.

664 [18]   McGraw PV, Walsh V, Barrett BT. Motion-Sensitive Neurones in V5/MT Modulate
665   Perceived Spatial Position. Current Biology 2004;14:1090–3.
666   doi:10.1016/j.cub.2004.06.028.

667 [19]   Maus GW, Fischer J, Whitney D. Motion-Dependent Representation of Space in Area
668   MT. Neuron 2013;78:554–62. doi:10.1016/j.neuron.2013.03.010.

669 [20]   Fischer J, Spotswood N, Whitney D. The emergence of perceived position in the visual
670   system. Journal of Cognitive Neuroscience 2011;23:119–36.
671   doi:10.1162/jocn.2010.21417.

672 [21]   Kriegeskorte N, Mur M, Bandettini PA. Representational similarity analysis -
673   connecting the branches of systems neuroscience. Front Syst Neurosci 2008;2.
674   doi:10.3389/neuro.06.004.2008.

675 [22]   Wagner AD, Maril A, Bjork RA, Schacter DL. Prefrontal Contributions to Executive
676   Control: fMRI Evidence for Functional Distinctions within Lateral Prefrontal Cortex.
677   NeuroImage 2001;14:1337–47. doi:10.1006/nimg.2001.0936.

678 [23]   Koechlin E, Ody C, Kouneiher F. The Architecture of Cognitive Control in the Human
679   Prefrontal Cortex. Science 2003;302:1181–5. doi:10.1126/science.1088545.

680 [24]   Dosenbach NUF, Fair DA, Miezin FM, Cohen AL, Wenger KK, Dosenbach RAT, et al.
681   Distinct brain networks for adaptive and stable task control in humans. Pnas
682   2007;104:11073–8. doi:10.1073/pnas.0704320104.

683 [25]   Dosenbach NUF, Fair DA, Cohen AL, Schlaggar BL, Petersen SE. A dual-networks
684   architecture of top-down control. Trends in Cognitive Sciences 2008;12:99–105.
685   doi:10.1016/j.tics.2008.01.001.

686 [26]   Bonini F, Burle B, Liégeois-Chauvel C, Régis J, Chauvel P, Vidal F. Action Monitoring
687   and Medial Frontal Cortex: Leading Role of Supplementary Motor Area. Science
688   2014;343:888–91. doi:10.1126/science.1247412.

689 [27]   Ridderinkhof KR, Ullsperger M, Crone EA, Nieuwenhuis S. The Role of the Medial
690   Frontal Cortex in Cognitive Control. Science 2004;306:443–7.
691   doi:10.1126/science.1100301.

692 [28]   Andersen RA, Essick GK, Siegel RM. Encoding of spatial location by posterior parietal
693   neurons. Science 1985;230:456–8. doi:10.1126/science.4048942.

694 [29]   Mishkin M, Ungerleider LG, Macko KA. Object vision and spatial vision: two cortical
695   pathways. Trends in Neurosciences 1983;6:414–7.

696 [30]   Badre D, Kayser AS, D'Esposito M. Frontal Cortex and the Discovery of Abstract
697   Action Rules. Neuron 2010;66:315–26. doi:10.1016/j.neuron.2010.03.025.

698 [31]   Badre D, Nee DE. Frontal Cortex and the Hierarchical Control of Behavior. Trends in
699   Cognitive Sciences 2018;22:170–88. doi:10.1016/j.tics.2017.11.005.

700 [32]   Hernández A, Nácher V, Luna R, Zainos A, Lemus L, Alvarez M, et al. Decoding a
701   Perceptual Decision Process across Cortex. Neuron 2010;66:300–14.
702   doi:10.1016/j.neuron.2010.03.031.

703 [33] Fried I, Mukamel R, Kreiman G. Internally Generated Preactivation of Single Neurons
704   in Human Medial Frontal Cortex Predicts Volition. Neuron 2011;69:548–62.
705   doi:10.1016/j.neuron.2010.11.045.

706 [34] Gallivan JP, McLean DA, Valyear KF, Pettypiece CE, Culham JC. Decoding Action
707   Intentions from Preparatory Brain Activity in Human Parieto-Frontal Networks. Journal
708   of Neuroscience 2011;31:9599–610. doi:10.1523/JNEUROSCI.0080-11.2011.

709 [35] Wallis G, Stokes M, Cousijn H, Woolrich M, Nobre AC. Frontoparietal and Cingulo-
710   opercular Networks Play Dissociable Roles in Control of Working Memory. Journal of
711   Cognitive Neuroscience 2015;27:2019–34. doi:10.1162/jocn_a_00838.

712 [36] Ploran EJ, Nelson SM, Velanova K, Donaldson DI, Petersen SE, Wheeler ME. Evidence
713   Accumulation and the Moment of Recognition: Dissociating Perceptual Recognition
714   Processes Using fMRI. Journal of Neuroscience 2007;27:11912–24.
715   doi:10.1523/JNEUROSCI.3522-07.2007.

716 [37] Andersen RA. Inferior Parietal Lobule Function in Spatial Perception and Visuomotor
717   Integration. vol. 52. Hoboken, NJ, USA: John Wiley & Sons, Inc; 2011.
718   doi:10.1002/cphy.cp010512.

719 [38] Jeannerod M, Arbib MA, Rizzolatti G, Sakata H. Grasping objects: the cortical
720   mechanisms of visuomotor transformation. Trends in Neurosciences 1995;18:314–20.
721   doi:10.1016/0166-2236(95)93921-J.

722 [39] Culham JC, Valyear KF. Human parietal cortex in action. Current Opinion in
723   Neurobiology 2006;16:205–12. doi:10.1016/j.conb.2006.03.005.

724 [40] Culham JC, Cavina-Pratesi C, Singhal A. The role of parietal cortex in visuomotor
725   control: What have we learned from neuroimaging? Neuropsychologia 2006;44:2668–
726   84. doi:10.1016/j.neuropsychologia.2005.11.003.

727 [41] McLelland D, Baker PM, Ahmed B, Bair W. Neuronal Responses during and after the
728   Presentation of Static Visual Stimuli in Macaque Primary Visual Cortex. Journal of
729   Neuroscience 2010;30:12619–31. doi:10.1523/JNEUROSCI.0815-10.2010.

730 [42] Whitney D, Goltz HC, Thomas CG, Gati JS, Menon RS, Goodale MA. Flexible
731   Retinotopy: Motion-Dependent Position Coding in the Visual Cortex. Science
732   2003;302:878–81. doi:10.2307/3835560?ref=search-
733   gateway:fdf31956690a23a49d1a5f4db92a3cf6.

734 [43] Kohler PJ, Cavanagh P, Tse PU. Motion-Induced Position Shifts Activate Early Visual
735   Cortex. Front Neurosci 2017;11:14. doi:10.3389/fnins.2017.00168.

736 [44] Whitney D, Cavanagh P. Motion distorts visual space: shifting the perceived position of
737   remote stationary objects. Nature Neuroscience 2000;3:954–9. doi:10.1038/78878.

738 [45] Silver MA, Ress D, Heeger DJ. Neural Correlates of Sustained Spatial Attention in
739   Human Early Visual Cortex. Journal of Neurophysiology 2007;97:229–37.
740   doi:10.1152/jn.00677.2006.

741 [46] de'Sperati C, Baud-Bovy G. Blind Saccades: An Asynchrony between Seeing and
742   Looking. Journal of Neuroscience 2008;28:4317–21. doi:10.1523/JNEUROSCI.0352-
743   08.2008.

744 [47] Schafer RJ, Moore T. Attention Governs Action in the Primate Frontal Eye Field.
745   Neuron 2007;56:541–51. doi:10.1016/j.neuron.2007.09.029.

746 [48] Zimmermann E, Morrone MC, Burr D. Visual motion distorts visual and motor space.
747   Journal of Vision 2012;12:10–0. doi:10.1167/12.2.10.

748 [49] van Heusden E, Rolfs M, Cavanagh P, Hogendoorn H. Motion Extrapolation for Eye
749   Movements Predicts Perceived Motion-Induced Position Shifts. Journal of Neuroscience
750   2018;38:8243–50. doi:10.1523/JNEUROSCI.0736-18.2018.
751 [50] Moore T, Zirnsak M. Neural Mechanisms of Selective Visual Attention.
752   Http://DxDoiorg/101146/Annurev-Psych-122414-033400 2017;68:47–72.
753   doi:10.1146/annurev-psych-122414-033400.
754 [51] Awh E, Armstrong KM, Moore T. Visual and oculomotor selection: links, causes and
755   implications for spatial attention. Trends in Cognitive Sciences 2006;10:124–30.
756   doi:10.1016/j.tics.2006.01.001.
757 [52] Mathworks I. MATLAB and statistics toolbox release 2012b. Natick (Massachusetts,
758   United States) 2012.
759 [53] Kleiner M, Brainard DH, Pelli D, Ingling A, Murray R, Broussard C. What's new in
760   Psychtoolbox-3 2007;36:1–16.
761 [54] Engel SA, Rumelhart DE, Wandell BA, Lee AT, Glover GH, Chichilnisky E-J, et al.
762   fMRI of human visual cortex. Nature 1994;369:525–5. doi:10.1038/369525a0.
763 [55] Sereno MI, Dale AM, Reppas JB, Kwong KK, Belliveau JW, Brady TJ, et al. Borders of
764   multiple visual areas in humans revealed by functional magnetic resonance imaging.
765   Science 1995;268:889–93. doi:10.1126/science.7754376.
766 [56] Huk AC, Dougherty RF, Heeger DJ. Retinotopy and Functional Subdivision of Human
767   Areas MT and MST. Journal of Neuroscience 2002;22:7195–205.
768   doi:10.1523/JNEUROSCI.22-16-07195.2002.
769 [57] Team RC. R: A language and environment for statistical computing 2013.
770 [58] Allaire J. RStudio: integrated development environment for R. Boston, MA 2012.
771 [59] Cox RW. AFNI: Software for Analysis and Visualization of Functional Magnetic
772   Resonance Neuroimages. Computers and Biomedical Research 1996;29:162–73.
773   doi:10.1006/cbmr.1996.0014.
774 [60] Talairach J, Tournoux P. Co-planar Stereotaxic Atlas of the Human Brain. George
775   Thieme Verlag; 1988.
776 [61] Fischl B, Sereno MI, Dale AM. Cortical Surface-Based Analysis: II: Inflation,
777   Flattening, and a Surface-Based Coordinate System. NeuroImage 1999;9:195–207.
778   doi:10.1006/nimg.1998.0396.
779 [62] Benjamini Y, Hochberg Y. Controlling the False Discovery Rate: A Practical and
780   Powerful Approach to Multiple Testing. Journal of the Royal Statistical Society Series B
781   (Methodological) 1995;57:289–300.
782 [63] Hanke M, Halchenko YO, Sederberg PB, Hanson SJ, Haxby JV, Pollmann S. PyMVPA:
783   a Python Toolbox for Multivariate Pattern Analysis of fMRI Data. Neuroinform
784   2009;7:37–53. doi:10.1007/s12021-008-9041-y.
785 [64] Stelzer J, Chen Y, Turner R. Statistical inference and multiple testing correction in
786   classification-based multi-voxel pattern analysis (MVPA): Random permutations and
787   cluster size control. NeuroImage 2013;65:69–82.
788   doi:10.1016/j.neuroimage.2012.09.063.
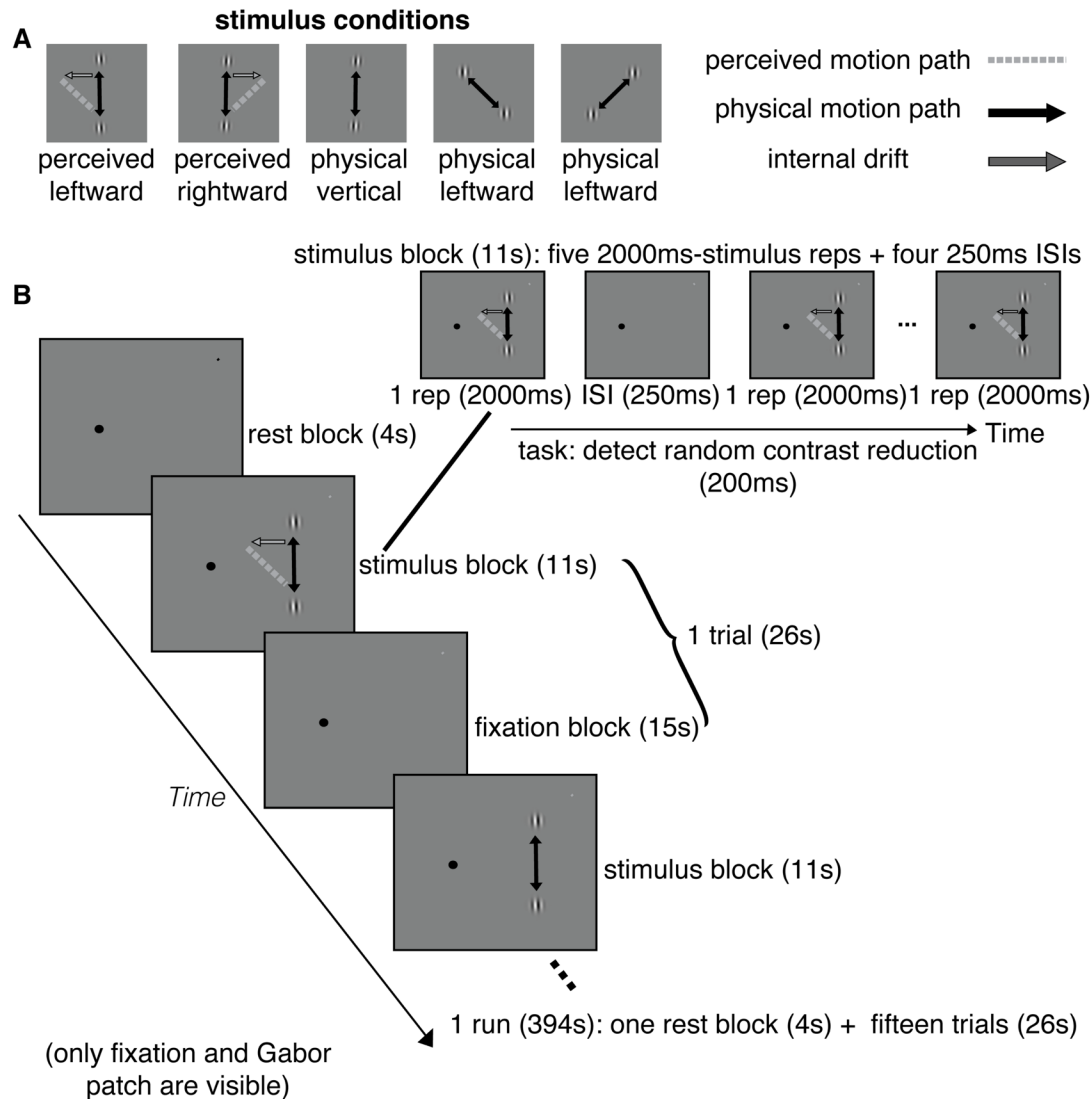789

Supplementary Information

Figure S1. Related to STAR Method. Stimulus conditions and study protocol of the main fMRI experiment.

(A) Stimulus conditions. The double-drift stimuli had a vertical physical motion path with opposite internal drift directions that could make the perceived motion path appear rotated either leftward or rightward relative to the physical motion path. The three control stimuli had either vertical, leftward or rightward physical motion paths with no internal drift.

(B) Main fMRI experiment protocol: Each run lasted 394s and started with a 4s fixation block followed by fifteen repetitions of 26s stimulus trials. Each trial was composed of an 11s stimulus block followed by a 15s fixation block. In each stimulus block, participants viewed a moving Gabor patch in the right hemifield (example shows a double-drift stimulus with leftward perceived motion path due to the internal drift) presented for 2s for a total of five repetitions with a 250 ms ISI in between repetitions. Participants were asked to detect a brief contrast reduction (200 ms) of the Gabor patch presented at a random moment during each trial.
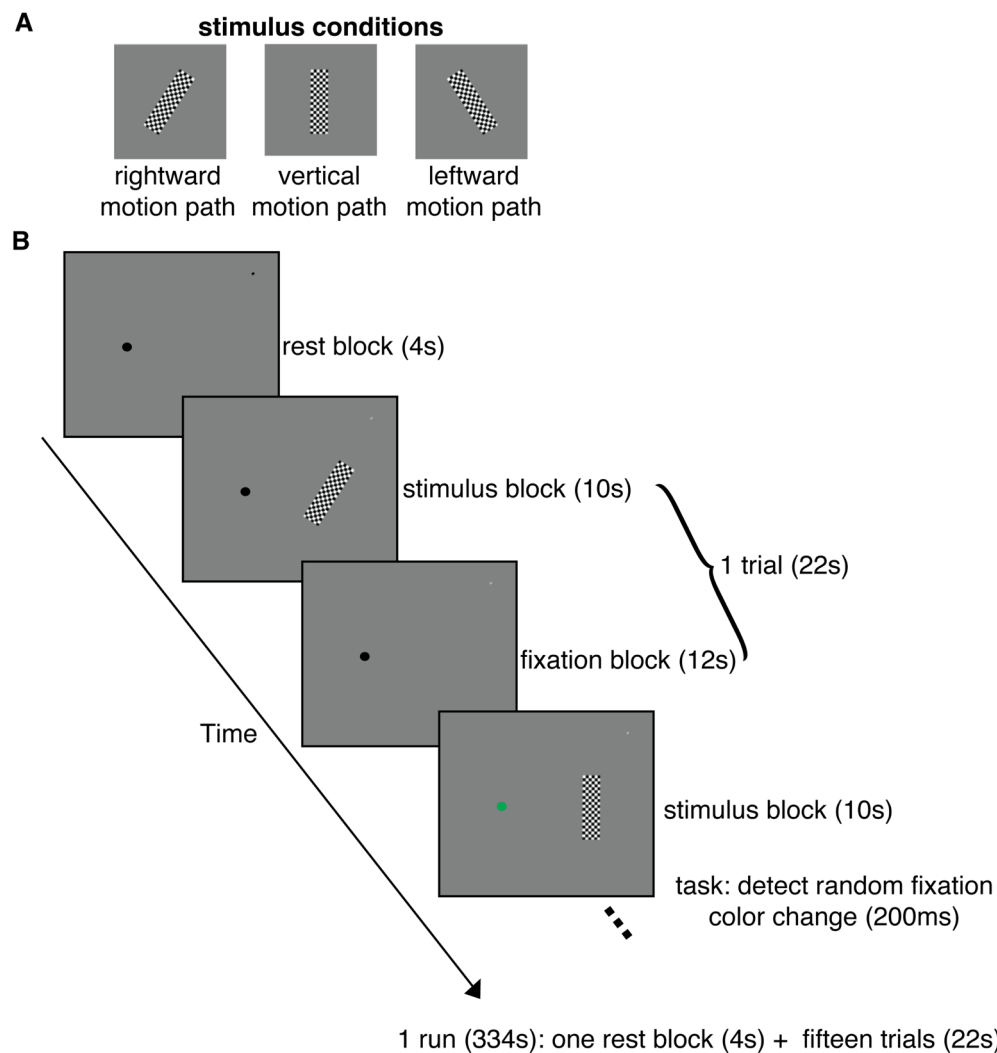
Figure S2. **Related to STAR Method. Stimulus conditions and study protocol of the fMRI localizer experiment.**

(A) Stimulus conditions. The checkboard pattern had three orientations that matched the physical (i.e. vertical motion path) or the measured perceived path orientation of the double-drift stimulus (i.e. rightward/leftward motion path).

(B) Each localizer run lasted 334s and started with a 4s rest block followed by fifteen stimulus trials (22s). Each trial was composed of a 10s-stimulus block with the stimulus flickered at 8 Hz followed by a 12s fixation block. Subjects were asked to detect random color changes (200 ms) of the fixation during the scan.
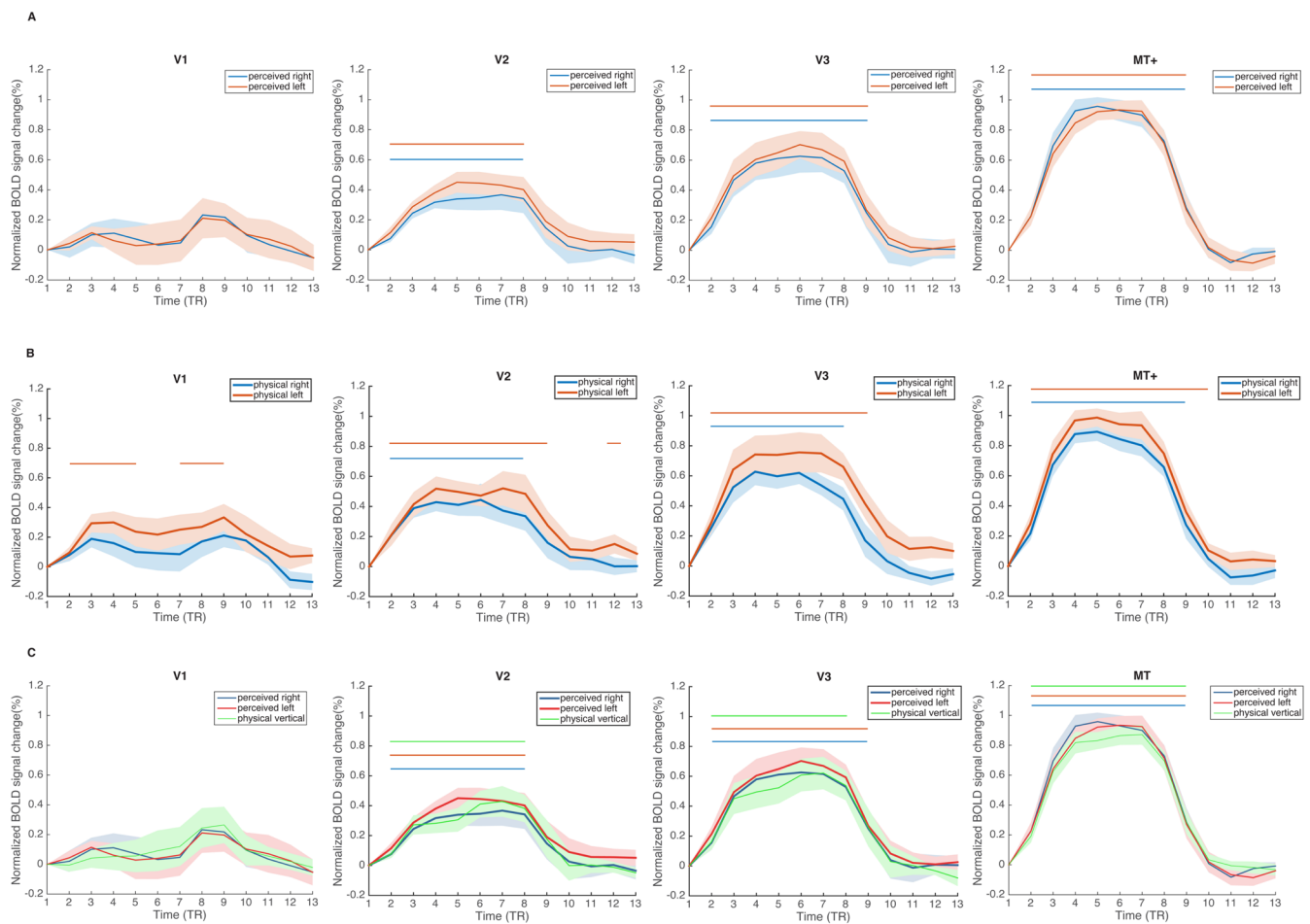
Figure S3. Related to Figure 3. Mean BOLD time course from MPROIs within V1, V2, V3 and MT+.
(A) two double-drift stimuli with perceived right vs. left but physically vertical motion directions.
(B) two control stimuli with matched physically right vs. left motion direction.
(C) two double-drift stimuli with internal motion that drives the perceived paths to appear leftward or rightward and the vertically moving control stimulus with no internal motion.
Error bars represents $\pm$ 1 SEM, horizontal lines at the top of each figure represent time points with significant above-baseline activity for each stimulus condition ($p < .05$). Paired samples t-tests showed no significant differences between the two double-drift stimulus conditions, the two control stimulus conditions, or between the double-drift stimuli (with internal motion) and control stimulus (with no internal motion) that shared the same physical (i.e. vertical) but different perceived motion direction (i.e. illusory left or right direction) (ps > .1).

■ trained on double-drift tested on control stimuli
■ trained control tested on double-drift stimuli
■ overlap
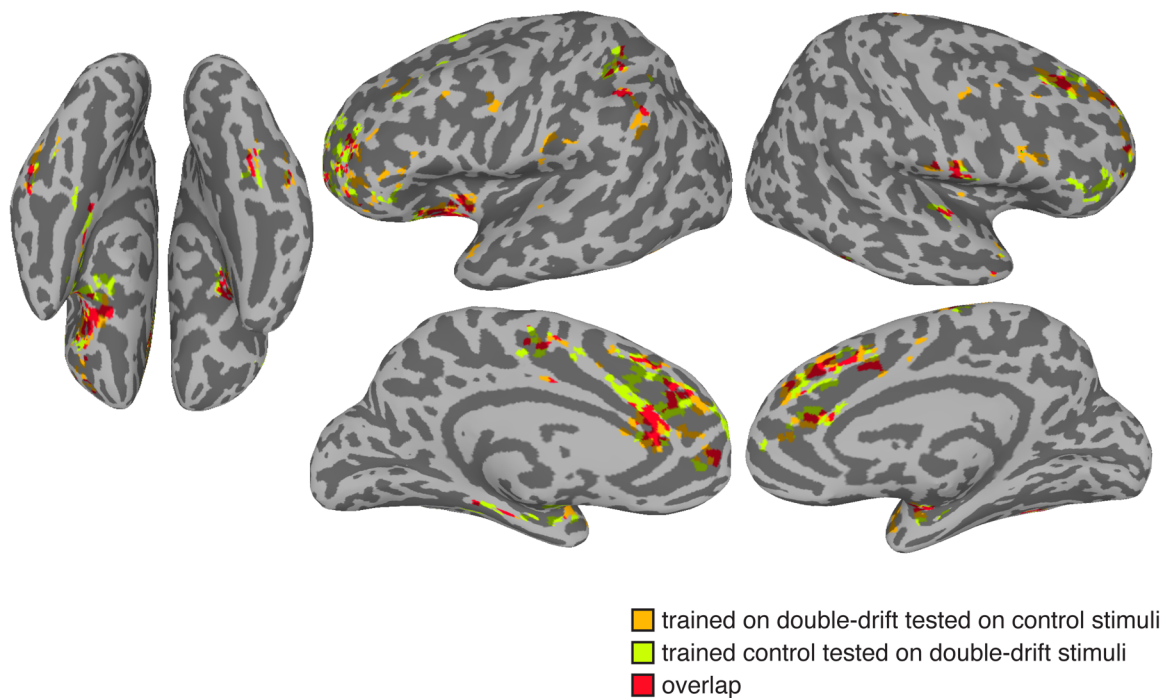
Figure S4. Related to Figure 6. Cluster-thresholded searchlight map with significant above-chance cross-decoding accuracy where the grand mean of each condition was removed within each searchlight during the analysis.
Orange represents significant clusters when training the classifier on double-drift and tested on the control stimuli. Green represents significant clusters when training the classifier on the control and tested on the double-drift stimuli. Results were thresholded at $p = .01$ and FDR corrected across clusters at $p < .05$.

Table S1. Related to Figure 3. Decoding performances and statistical results in each MPROI.

ROI Name	Size ± SEM (voxels)	Decoding condition	Mean decoding accuracy ± SEM (%)	FDR-adjusted p
V1	72 ± 14	Illusory paths	50.6 ± 5.6	0.435
		Physical paths	90.6 ± 4.4	0
		Illusory to matched physical paths	45 ± 4.1	0.93
		Matched physical to illusory paths	47.8 ± 1.9	0.73
V2	112 ± 22	Illusory path	60 ± 2.6	0.004
		Physical paths	86.7 ± 5.1	0
		Illusory to matched physical paths	53.5 ± 5.7	0.82
		Matched physical to illusory paths	50.6 ± 4.9	0.73
V3	141 ± 70	Illusory path	60 ± 3.7	0
		Physical paths	78.9 ± 4.3	0
		Illusory to matched physical paths	51.1 ± 7.9	0.82
		Matched physical to illusory paths	48.9 ± 5.1	0.73
MT+	194 ± 71	Illusory path	53.9 ± 2.3	0.12
		Physical paths	62.2 ± 2.8	0
		Illusory to matched physical paths	52.2 ± 3.2	0.82
		Matched physical to illusory paths	56.7 ± 3.7	0.19

Table S2. Related to Figure 5. Significant clusters found in the within-condition classification searchlight analysis (thresholded at $p = 0.01$ and FDR-corrected across clusters at $p < 0.05$).

Decoding condition	Size (voxels)	Peak				areas
		MNI coordinates			Classification accuracy (%)	
		X	Y	Z		
Illusory path	4720	13.5	-31.5	2.5	73.3	Superior frontal gyrus, medial frontal gyrus, anterior cingulate, right parahippocampal gyrus, right superior temporal gyrus
	2993	-10.5	58.5	-12.5	72.2	Middle occipital gyri, right precuneus, right parahippocampal gyrus, right angular gyrus
	1713	22.5	10.5	29.5	72.2	Left cingulate gyrus, left postcentral gyrus
	294	-19.5	19.5	29.5	68.9	Right cingulate gyrus
	220	34.5	1.5	-21.5	71.1	Left parahippocampal gyrus, left superior temporal gyrus
Matched physical path	21761	13.5	85.5	8.5	85.5	Left middle occipital gyrus, superior and middle temporal gyri, left inferior parietal lobule, superior and middle frontal gyri, precentral gyri, postcentral gyri, paracentral lobule, cingulate gyri

Table S3. Related to Figure 6. Significant clusters found in the cross-decoding searchlight analysis (thresholded at $p = 0.01$ and FDR-corrected across clusters at $p < 0.05$).

Decoding condition	Size (voxels)	Peak decoding accuracy				areas
		MNI coordinates			Classification accuracy (%)	
		X	Y	Z		
Trained on double-drift tested on control stimuli	1670	7.5	-34.5	26.5	67.2	right superior frontal gyrus, medial frontal gyri, anterior cingulate
	441	4.5	22.5	2.5	65	Left thalamus
	204	31.5	46.5	26.5	65.6	Left inferior parietal lobule
	168	-49.5	-1.5	47.5	64.4	Right precentral gyrus, right middle frontal gyrus
	120	43.5	-1.5	35.5	63.3	Left precentral gyrus, left middle frontal gyrus
	86	-40.5	-28.5	-3.5	65	Right inferior frontal gyrus
	78	37.5	46.5	-24.5	64	Left cerebellum
	48	40.5	64.5	29.5	61.7	Left angular gyrus
Trained on control tested on double-drift stimuli	603	-7.5	-22.5	26.5	65	medial frontal gyri, anterior cingulate
	148	34.5	-49.5	23.5	62.8	Left superior frontal gyrus
	134	25.5	37.5	47.5	63.3	Left postcentral gyrus
	131	7.5	28.5	-3.5	63.9	Left thalamus
	60	22.5	31.5	-21.5	61.1	Left cerebellum
	50	-37.5	-4.5	-21.5	62.8	Right superior temporal gyrus, right parahippocampal gyrus
	49	-61.5	10.5	20.5	61.7	Right precentral gyrus
	47	-43.5	-37.5	-3.5	61.7	Right inferior frontal gyrus
	36	22.5	-1.5	-12.5	61.1	Left parahippocampal gyrus
	33	-13.5	19.5	59.5	61.7	Right precentral gyrus
	30	-4.5	-52.5	23.5	60	Right superior frontal gyrus

Table S4. Related to Figure 6. Significant clusters found in the cross-decoding searchlight analysis where the grand mean of each condition was removed within each searchlight during the analysis (thresholded at $p = 0.01$ and FDR-corrected across clusters at $p < 0.05$).

Decoding condition	Size (voxels)	Peak decoding accuracy				areas
		MNI coordinates			Classification accuracy (%)	
		X	Y	Z		
Trained on double-drift tested on control stimuli	517	-19.5	-46.4	23.5	64.4	right superior frontal gyrus, right medial frontal gyri
	402	19.5	-46.5	-0.5	65.6	Left anterior cingulate, left superior frontal gyrus
	185	31.5	40.5	35.5	64.4	Left inferior parietal lobule
	145	-25.5	4.5	-15.5	61.7	Right parahippocampal gyrus
	119	-40.5	49.5	-36.5	63.9	Right cerebellum
	89	-10.5	13.5	65.5	64.4	Right superior frontal gyrus, right medial frontal gyrus
	82	4.5	31.5	2.5	64.4	Left thalamus
	75	46.5	49.5	-24.5	66.1	Left cerebellum
	75	-49.5	-13.5	41.5	62.2	Right middle frontal gyrus
	46	-10.5	-31.5	8.5	61.7	Right anterior cingulate
	45	-16.5	-37.5	5.5	61.7	Right anterior cingulate, right medial frontal gyrus
	44	-61.5	10.5	20.5	61.7	Right postcentral gyrus
	34	46.5	-4.5	32.5	61.7	Left inferior frontal gyrus, left precentral gyrus
	31	10.5	19.5	-12.5	62.2	Left parahippocample gyrus
Trained on control tested on double-drift stimuli	504	34.5	-52.5	11.5	66.1	Left middle frontal gyrus, left superior frontal gyrus
	487	-13.5	-28.5	38.5	65.6	Right medial frontal gyrus
	161	13.5	25.5	-12.5	63.9	Left cerebellum
	121	28.5	43.5	32.5	63.9	Left inferior parietal lobule
	112	22.5	-19.5	-9.5	63.3	Left inferior frontal gyrus
	108	-49.5	-34.5	11.5	63.3	Right inferior frontal gyrus
	81	-25.5	1.5	-15.5	64.4	Right parahippocampal gyrus
	53	-22.5	-52.5	14.5	62.2	Right superior frontal gyrus
	48	22.5	13.5	-15.5	61.7	Left parahippocampal gyrus
	42	52.5	43.5	41.5	64.4	Left inferior parietal lobule
	41	-10.5	16.5	59.5	65.6	Right medial frontal gyrus
	38	-58.5	7.5	17.5	63.3	Right postcentral gyrus
	33	10.5	-13.5	56.5	61.7	Left superior frontal gyrus
	32	7.5	10.5	44.5	61.1	Left paracentral lobule

	30	-31.5	37.5	-18.5	61.1	Right cerebellum

KEY RESOURCES TABLE

	SOURCE	IDENTIFIER
Software and Algorithms		
MATLAB 2015a	MathWorks [52]	https://www.mathworks.com/
AFNI	[59]	https://afni.nimh.nih.gov/
FreeSurfer	[61]	http://surfer.nmr.mgh.harvard.edu
Psychophysics Toolbox	[53]	https://psychtoolbox.com/
R version 3.3.2, RStudio interface	[57,58]	https://www.r-project.com/
PyMVPA	[63]	http://www.pymvpa.org/